Network Phases in ABC Triblock Copolymers

Thomas H. Epps, III,† Eric W. Cochran,†
Cordell M. Hardy, Travis S. Bailey,
Ryan S. Waletzko, and Frank S. Bates*

Department of Chemical Engineering and Materials Science, University of Minnesota, Minneapolis, Minnesota 55455

Received April 2, 2004
Revised Manuscript Received July 13, 2004

Many naturally occurring and engineered products are influenced by network structures. Collagen networks provide a scaffold for living tissue, while swollen arrays of physically cross-linked polypeptides constitute gelatin, the familiar dessert and electrophoresis medium. Although the associated mesh sizes differ by several orders of magnitude, these examples share a common feature: three-dimensional connectivity that imparts mechanical rigidity. Intercalating additional interconnected components can yield broader functions, e.g., ionic or electrical conductivity, optical band gaps, and tailored heat and mass transfer.[1−3]

At mesoscopic length scales (between roughly one nanometer and one micron) interfacial curvature and packing geometry often reflect self-assembly of molecules endowed with prescribed architectures and directed interactions.[4] Under the appropriate conditions, hydrated soaps, lipids, and surfactants form soft, permeable, bicontinuous solids,[5−7] some capable of templating hard mesoporous ceramic networks.[8,9] Block copolymers provide even greater flexibility in manipulating the precise placement of engineering materials in a plethora of nanoscale configurations.[10,11] However, aside from linear permutations of two block types (AB, ABA, ABAB, etc.) there is currently no reliable way to anticipate block copolymer morphologies from theory.

This communication summarizes a comprehensive investigation of a homologous set of linear poly(isoprene-*b*-styrene-*b*-ethylene oxide) (ISO) triblock copolymers. We have synthesized and characterized more than eighty ISO triblock copolymers over the past 4 years, covering a wide range of compositions. Here we focus on a total of 43 model compounds ($M_w/M_n < 1.08$) with molecular weights $15 < M_w < 25$ kg/mol and compositions bounded by $0.20 \le f_I \le 0.58$, $0.25 \le f_S \le 0.58$, and $0 \le f_O \le 0.37$, where f_i is the volume fraction of block i, calculated from the experimentally determined weight fractions and published homopolymer densities at 140 °C: $\rho_I = 0.830$, $\rho_S = 0.969$, and $\rho_O = 1.064$ g/mol.[12] The associated phases are identified in the triangular phase portrait illustrated in Figure 1.

The experiments described here were conducted above 100 °C, which exceeds the melting ($T_{m,O} \cong 65$ °C) and glass transition ($T_{g,S} \cong 90$ °C) temperatures. Most of the block copolymers exhibited an order−disorder transition temperature (T_{ODT}) above 100 °C, and generally below 250 °C. Ordered phases have been identified using a complement of four techniques: small-angle X-ray scattering (SAXS) performed at the Advanced Photon Source (APS, Argonne National Laboratory) or the University of Minnesota, transmission electron microscopy (TEM), light depolarization (birefringence), and dynamic mechanical spectroscopy (DMS).

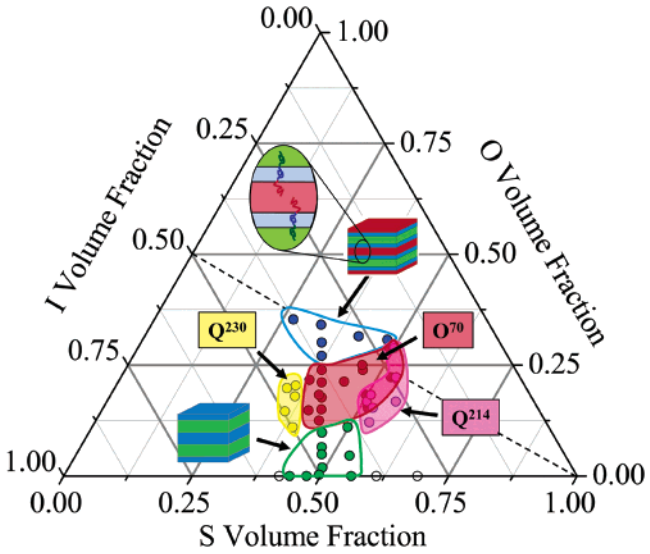

Figure 1. Poly(isoprene-*b*-styrene-*b*-ethylene oxide) (ISO) phase portrait in the vicinity of the order−disorder transition temperature. Filled and open circles indicate ordered and disordered states within the experimental temperature range $100 \le T \le 225$ °C. Shaded areas identify compositions with two- and three-domain lamellae (identified by sketches), and three network phases, Q^{230}, O^{70}, and Q^{214}. Overlap of the O^{70} and Q^{214} phase boundaries indicates high and low temperature occurrence, respectively, of each phase. The dashed line identifies the condition $f_I = f_O$, associated with symmetric ISO molecules.

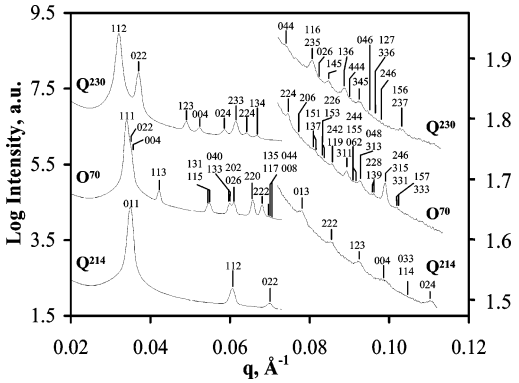

Figure 2. SAXS data obtained from ISO specimens located within each of the three network phases. Samples were prepared by cooling from above T_{ODT} followed by annealing and measurement at 150 °C. Scattering patterns labeled Q^{230} and Q^{214} are uniquely indexed by the cubic space groups $Ia\bar{3}d$ and $I4_132$, respectively. Scattering from O^{70} is indexed based on *Fddd* space group symmetry. Data for $q > 0.7$ Å^{-1} is presented according to a different intensity scale (right axis) so that higher order reflections are visible. Compositions (I/S/O) for the Q^{230}, Q^{214}, and O^{70} samples are 0.47/0.33/0.20, 0.33/0.51/0.16, and 0.41/0.41/0.18, respectively.

Previous experiments with a subset of the ISO polymers, located on the isopleth defined by $f_I = f_S$, indicated that a triply continuous network phase (tentatively associated with *Fddd* space group symmetry) separated the two-domain (I and S) and three-domain (I, S, and O) lamellar states.[13] A representative SAXS powder pattern, obtained from a specimen located in the composition window labeled O^{70} (see Figure 1), is

* To whom correspondence should be addressed. E-mail: bates@cems.umn.edu.
† These authors contributed equally to this work.

10.1021/ma0493426 CCC: $27.50
Published on Web 08/19/2004

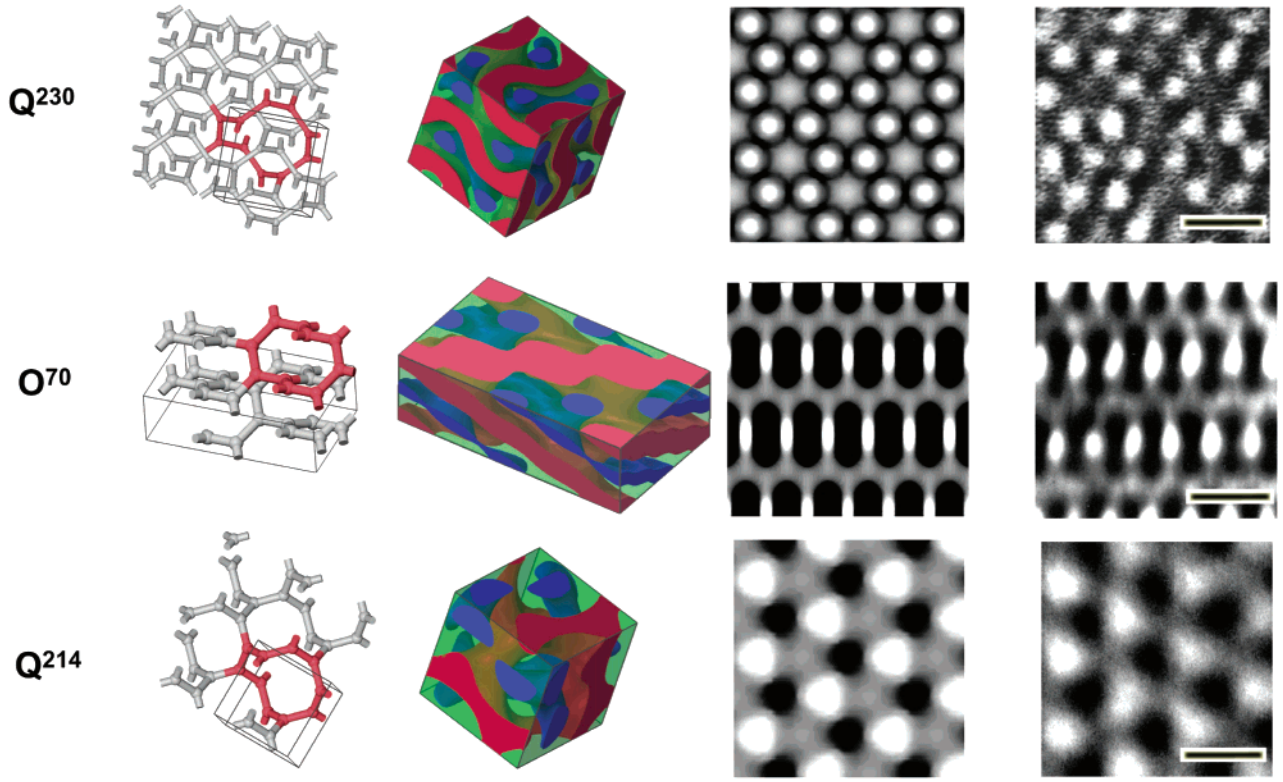

Figure 3. Network lattice structures, 3-D morphologies and 2-D projections derived from level set constructions, and TEM images from network phases Q^{230}, O^{70}, and Q.[214] Double (Q^{230}), and single (Q^{214}, O^{70}) networks, each constructed from 10-node three-connector loops (highlighted) were deduced from SAXS based space group assignments. Level set surfaces, constrained by the block copolymer composition, result in 3-D morphologies containing I (blue), S (green), and O (red) domains. Gray scale shading and projection to 2-dimensions ([111] and [110] directions for the cubic and orthorhombic systems, respectively) connects the SAXS data and TEM images. ISO specimens were stained with osmium tetraoxide. Agreement between the calculated and experimental images supports the morphology assignments. The scale bars in the TEM images represent 30 nm.

presented in Figure 2; intensity is plotted vs scattering wavevector modulus, $|\mathbf{q}| = 4\pi\lambda^{-1}\sin(\theta/2)$, where λ is the X-ray wavelength, and θ is the scattering angle. At least 13 reflections can be identified, and indexed with *Fddd* symmetry, yielding an orthorhombic unit cell with dimensions $a = 0.305c$, $b = 0.586c$, $c = 71.4$ nm; these lattice parameters vary slightly with composition. Single crystal (2-D) SAXS diffraction provides additional confirmation of this phase assignment.[14] Following an established convention,[15] we refer to this phase as O^{70}, representing the Bravais lattice and space group (No. 70).

Two other complex phases, denoted Q^{230} and Q^{214}, have been discovered on either side of the O^{70} phase. Representative SAXS powder patterns, included in Figure 2, are both consistent with cubic ordering. The first 11 reflections (and higher order peaks) evident in the data labeled Q^{230} coincide uniquely with the first 11 allowed reflections for the $Ia\bar{3}d$ space group (No. 230). Furthermore, the ratio of first to second peak intensities, $I_{112}/I_{220} \approx 10$, is consistent with the familiar gyroid structure.[16,17] Triblocks from the region in Figure 1 denoted Q^{214} also produced exceptional SAXS patterns with reflections located at $q/q^* = 1, \sqrt{3}, \sqrt{4}, \sqrt{5}, \sqrt{6}, \sqrt{7}, \sqrt{8}$, and $\sqrt{10}$, where q^* is the primary peak location. Absence of diffraction at $\sqrt{2}q^*$ eliminates all but the $I4_132$ space group (No. 214), which we assign to this phase.[18] Both the O^{70} and Q^{214} phases were documented in individual specimens at compositions where the phase boundaries overlap (see below).

The three space groups identified by SAXS are associated with three network structures, each formed by joining planar trivalent connectors into 10-node loops arranged on a 3-dimensional lattice. Following Wells' notation, we refer to these as (10,3) networks.[19] $I4_132$ supports a single, chiral, (10,3)*a* network, formed from symmetric 3-fold connectors. A double network with $Ia\bar{3}d$ symmetry is created by intercalation of exactly balanced (10,3)*a* enantiomers. The centrosymmetric (10,3)*c* network, created from connectors with mirror plane symmetry, has *Fddd* symmetry. Figure 3 (first column) illustrates each of these lattices, and highlights the (10,3) loop building blocks.

Adding block copolymers to a specific lattice produces a space filling morphology. We have employed level sets, mathematical surfaces that partition space according to the space group operations derived from the SAXS patterns, to approximate the three-dimensional morphologies associated with the postulated networks.[20,21] When constrained by the experimental compositions, these surfaces closely mimic the actual interfacial topology, and the resulting 3-D images provide useful real-space depictions of the network morphologies (Figure 3, second column). 2-D projections of these structures, along [111] and [110] directions of the cubic and orthorhombic morphologies, respectively, are illustrated in Figure 3 (third column). Black (I) and white (S and O) shading levels were assigned to the I, S, and O domains, simulating the TEM contrast obtained when ISO is stained with osmium tetroxide.[13] Correspondence of these level set projections (patterns, and absolute length scales derived from SAXS) and OsO_4-stained TEM images (Figure 3, fourth column) lead us to conclude that the Q^{214} and Q^{230} phases contain tricon-

tinuous and pentacontinuous forms of the gyroid morphology, respectively, while the O^{70} phase represents a tricontinuous orthorhombic network.

Here we note that the sharp interfaces defined by the solid domain models in Figure 3 (second column) are not an accurate physical interpretation of the monomer density profile. Instead, they more closely approximate an imaginary boundary that delimits A-*rich* domains from B-rich, etc.... The polymers considered in this communication were all prepared in the weak-to-intermediate segregation regime, which results not in discrete block domains but instead smoothly varying periodic composition fields, the symmetry of which define the morphology. Thus, our usage of "two-domain" and "three-domain" in the remaining discussion serves only as a conceptual construct that delimits the two regions of lamellae on O-lean and O-rich sides of the network region.

The network forming materials exhibit two distinct optical properties: Q^{214} and Q^{230} are optically isotropic, while O^{70} is birefringent.[13] We have exploited this difference in characterizing the $Q^{214}-O^{70}$ order−order transition (OOT) in samples located in the boundary region found in Figure 1. Specimens were held between crossed polarizing films, and the intensity of transmitted light was monitored while heating or cooling at 1 °C/min (Figure 4, lower panel). At the highest temperatures, in the disordered state, only a baseline signal was recorded. Growth of the O^{70} phase upon cooling resulted in substantial birefringence, while the transition to Q^{214} returned the signal to the baseline level. Heating reversed this trend, with a 10−15 °C hysteretic lag, evidence of a symmetry breaking first-order phase transition. The symmetry of each phase was established with static SAXS measurements. These facile and reversible network transitions lead to the conclusion that Figure 1 represents equilibrium phase behavior.

The upper panel of Figure 4 illustrates the linear dynamic shear modulus, G', obtained while heating and cooling (1 °C/min) through the $Q^{214}-O^{70}$ and O^{70}–disorder transitions. Transition from disorder to order is accompanied by a large, hysteretic change in elasticity,[22] while the transition between network phases is nearly imperceptible, consistent with the triply periodic (i.e., solid) phase assignments.

Although Q^{230}, O^{70}, and Q^{214} each have been described previously,[13,17,18] to the best of our knowledge no two 3-D network morphologies have been reported in a homologous set of triblock copolymers.

Phase complexity increases dramatically with the number of thermodynamically incompatible blocks. A single A/B interface partitions linear AB diblocks into four equilibrium morphologies: spheres, cylinders, lamellae and the Q^{230} gyroid.[23,24] One additional block triples the number of possible interfaces (e.g., A/B, B/C, and A/C), complicating the free energy competition that dictates phase formation. At least two-dozen structures have been documented in linear ABC triblocks.[25−28]

Interfacial tension between amorphous polymers is governed by the Flory−Huggins parameter: $\gamma_{ij} \propto \sqrt{\chi_{ij}}$. For ISO the associated binary interactions, $\chi_{IS} \approx \chi_{SO} < \chi_{IO}$, favor morphologies with two interfaces: I/S and S/O. (Inverting this sequence to SIO results in morphologies with three interfaces for certain compositions).[29] Symmetric compositions produce two-domain ($f_I \approx f_S$; $f_O \approx 0$) and three-domain ($f_I \approx f_S \approx f_O$) lamellae with flat interfaces (see sketches in Figure 1). Adding an asymmetric O block to a symmetric IS diblock destabilizes the lamellar geometry. Chain packing at the S/O interface unbalances the space filling requirements at the nominally symmetric I/S interface, buckling the layers and producing hyperbolic (saddle) interfacial surfaces, a distinguishing feature of the network morphologies. This notion motivated our interest in exploring the composition region between two- and three-domain lamellae.[21,30] Apparently, trifunctional connectors, rather than 4- or 6-fold types, best accommodate single component linear block copolymer melts at compositions and χ_{ij}'s where network formation is favored. However, molecular branching, or blending with homopolymers or other diluents, can relax this constraint.[31]

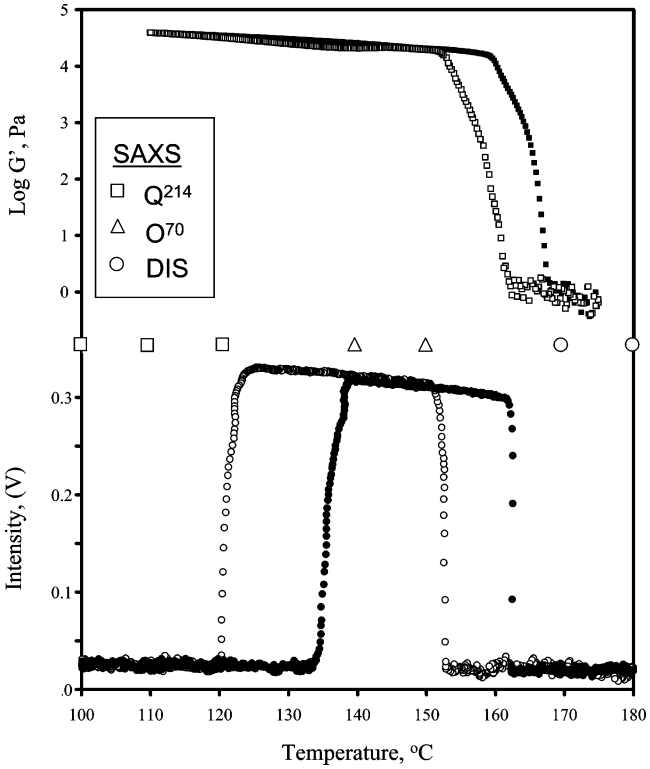

Figure 4. Physical properties of an ISO sample (0.25/0.53/0.22) located in the O^{70}/Q^{214} overlap region in Figure 1. Linear dynamic elastic shear modulus G' (■, □) and light depolarization (●, ○) were determined while heating (■, ●) and cooling (□, ○) at 1 °C/min. Isothermal SAXS measurements identify the Q^{214} and O^{70} network phases, and disorder (DIS), at several temperatures. Depolarization of light (birefringence) at intermediate temperatures is consistent with orthorhombic (O^{70}) symmetry, while the absence of optical activity at higher and lower temperatures supports assignments of disorder and cubic (Q^{214}) symmetry, respectively. Invariance in G', while heating and cooling through Q^{214} and O^{70}, is consistent with the triply periodic network assignments. Hysteresis in the G' and birefringence measurements upon heating and cooling is indicative of first-order phase transitions.

The Q^{214} phase was first predicted with self-consistent mean field theory in the limit of symmetric interactions ($\chi_{AB} \approx \chi_{BC} < \chi_{AC}$),[32] and subsequently identified in poly(isoprene-*b*-styrene-*b*-vinylpyridine) (ISV) triblock copolymers.[18] Increasing the length of equal size end blocks in an ABC triblock (i.e., $f_A = f_C$, dashed line in Figure 1) leads to a sequence of phase transitions, from alternating A and C spheres, to alternating cylinders, then the Q^{214} gyroid, and finally three-domain lamellae.[33] The location of the Q^{214} and three-domain lamellar phases in Figure 1 nearly coincides with these prior treatments. (Minor variations in the composition de-

pendence of each phase can be attributed to second-order effects such as differences in the statistical segment length of individual blocks.[34])

At the opposite end of the network channel lies the Q^{230} phase. The associated double lattice accommodates two pairs of parallel I/S and S/O interfaces, defining five independent continuous domains: one I, two S, and two O (see Figure 3). This pentacontinuous phase was first identified in ISD triblock copolymers (D refers to poly(dimethylsiloxane)),[17] and subsequently in SIO,[29] and several block copolymer blends.[35] Surprisingly, all prior examples of the pentacontinuous Q^{230} phase are characterized by asymmetric interactions ($\chi_{AB} \approx \chi_{AC} < \chi_{BC}$). Obviously this is not a prerequisite since $\chi_{AB} \approx \chi_{BC} < \chi_{AC}$ for ISO.

Between the two cubic phases, and bounded by the two- and three-domain lamellar states, lies the most expansive region in the network channel, the orthorhombic O^{70} phase. This relatively low symmetry structure reflects a fascinating compromise between the interfacial tension and area and the chain stretching across three blocks. Locally, O^{70} resembles Q^{214} each is formed from a single network lattice with trifunctional nodes. To our knowledge O^{70} is the only non-cubic network phase found in self-assembling soft materials. This unusual structure seems to embody a new type of frustrated self-assembly.

Unraveling the specific factors responsible for the phase behavior shown in Figure 1 will require fresh theoretical insights. The block sequence, composition, and molecular weight dependences of these phases are not anticipated by current treatments. Adding just one C block to the well-understood AB architecture has (at least) tripled the number of equilibrium network phases. Increasing architectural complexity through the addition of more blocks and other linear sequences (e.g., ABCBA, ABCAB, ABCD, etc.), and through branching, it may yield even more complex network phases.

Acknowledgment. This work was supported by the NSF through Grant DMR-0220460. Graduate fellowships to T.H.E. (Lucent Technologies), E.W.C. (NSF), and C.M.H. (NSF) are gratefully acknowledged. Use of the Advanced Photon Source was supported by the U.S. Department of Energy, Basic Energy Sciences, Office of Science, under Contract No. W-31-109-Eng-38. This research program has made extensive use of the MRSEC (NSF) supported Institute of Technology Characterization Facility at the University of Minnesota.

References and Notes

(1) Subramanian, G.; Manoharan, V. N.; Thorne, J. D.; Pine, D. J. *Adv. Mater. (Weinheim, Ger.)* **1999**, *11*, 1261−1265.
(2) Edrington, A. C.; Urbas, A. M.; DeRege, P.; Chen, C. X.; Swager, T. M.; Hadjichristidis, N.; Xenidou, M.; Fetters, L. J.; Joannopoulos, J. D.; Fink, Y.; Thomas, E. L. *Adv. Mater. (Weinheim, Ger.)* **2001**, *13*, 421−425.
(3) Keil, F. *Chem. Tech. (Leipzig, Germ.)* **1992**, *44*, 357−363.
(4) Whitesides, G. M.; Grzybowski, B. *Science* **2002**, *295*, 2418−2421.
(5) Scriven, L. E. *Nature (London)* **1976**, *263*, 123−125.
(6) Duesing, P. M.; Templer, R. H.; Seddon, J. M. *Langmuir* **1997**, *13*, 351−359.
(7) Landh, T. *FEBS Lett.* **1995**, *369*, 13−17.
(8) Kresge, C. T.; Leonowicz, M. E.; Roth, W. J.; Vartuli, J. C.; Beck, J. S. *Nature (London)* **1992**, *359*, 710−712.
(9) Simon, P. F. W.; Ulrich, R.; Spiess, H. W.; Wiesner, U. *Chem. Mater.* **2001**, *13*, 3464−3486.
(10) Muthukumar, M.; Ober, C. K.; Thomas, E. L. *Science* **1997**, *277*, 1225−1232.
(11) Ruokolainen, J.; Makinen, R.; Torkkeli, M.; Makela, T.; Serimaa, R.; ten Brinke, G.; Ikkala, O. *Science* **1998**, *280*, 557−560.
(12) Fetters, L. J.; Lohse, D. J.; Ritcher, D.; Witten, T. A.; Zirkel, A. *Macromolecules* **1994**, *27*, 4639−4646.
(13) Bailey, T. S.; Hardy, C. M.; Epps, T. H., III.; Bates, F. S. *Macromolecules* **2002**, *35*, 7007−7017.
(14) Epps, T. H., III.; Cochran, E. W.; Waletzko, R. S.; Bailey, T. S.; Hardy, C. M.; Bates, F. S. **2004**, manuscript in review.
(15) Seddon, J. M. *Biochim. Biophys. Acta* **1990**, *1031*, 1−69.
(16) Schulz, M. F.; Bates, F. S.; Almdal, K.; Mortensen, K. *Phys. Rev. Lett.* **1994**, *73*, 86−89.
(17) Shefelbine, T. A.; Vigild, M. E.; Matsen, M. W.; Hajduk, D. A.; Hillmyer, M. A.; Cussler, E. L.; Bates, F. S. *J. Am. Chem. Soc.* **1999**, *121*, 1, 8457−8465.
(18) Suzuki, J.; Seki, M.; Matsushita, Y. *J. Chem. Phys.* **2000**, *112*, 4862−4868.
(19) Wells, A. F. *Three-Dimensional Nets and Polyhedra*; John Wiley & Sons: New York, 1977.
(20) Mermin, N. D. *Rev. Mod. Phys.* **1992**, *64*, 3−49.
(21) Wohlgemuth, M.; Yufa, N.; Hoffman, J.; Thomas, E. L. *Macromolecules* **2001**, *34*, 6083−6089.
(22) Rosedale, J. H.; Bates, F. S. *Macromolecules* **1990**, *23*, 2329−2338.
(23) Khandpur, A. K.; Foster, S.; Bates, F. S.; Hamley, I. W.; Ryan, A. J.; Bras, W.; Almdal, K.; Mortensen, K. *Macromolecules* **1995**, *28*, 8796.
(24) Matsen, M. W.; Bates, F. S. *Macromolecules* **1996**, *29*, 1091−1098.
(25) Auschra, C.; Stadler, R. T. *Macromolecules* **1993**, *26*, 2171−2174.
(26) Mogi, Y.; Nomura, M.; Kotsuji, H.; Ohnishi, K.; Matsushita, Y.; Noda, I. *Macromolecules* **1994**, *27*, 6755−6760.
(27) Bates, F. S.; Fredrickson, G. H. *Phys. Today* **1999**, *52*, 32−38.
(28) Abetz, V.; Bayreuth University: Bayreuth, Germany, 2000.
(29) Bailey, T. S.; Pham, H. D.; Bates, F. S. *Macromolecules* **2001**, *34*, 6994−7008.
(30) Matsen, M. W.; Bates, F. S. *Macromolecules* **1996**, *29*, 7641−7644.
(31) Finnefrock, A. C.; Ulrich, R.; Toombes, G. E. S.; Gruner, S. M.; Wiesner, U. *J. Am. Chem. Soc.* **2003**, *125*, 13084−13093.
(32) Matsen, M. W. *J. Chem. Phys.* **1998**, *108*, 785−796.
(33) Mogi, Y.; Kotsuji, H.; Kaneko, Y.; Mori, K.; Matsushita, Y.; Noda, I. *Macromolecules* **1992**, *25*, 5408−5411. The initial diamond assignment was corrected in ref 18.
(34) Matsen, M. W.; Bates, F. S. *J. Polym. Sci., Part B: Polym. Phys.* **1997**, *35*, 945−952.
(35) Goldacker, T.; Abetz, V. *Macromol. Rapid Commun.* **1999**, *21*, 16.

MA0493426